Self-Mixing Displacement Measured by a Two-Color Laser in 66-nm Steps

Silvano Donati, *Life Fellow, IEEE*, Riccardo Gotti, Antonio Agnesi, and Federico Pirzio

***Abstract*— We demonstrate a new self-mixing interferometer (SMI) simultaneously working on two wavelengths, the fundamental at 1064 nm and the second harmonic at 532 nm delivered in the same beam. The beam is sent to the remote target in the usual way, and in the return path, two photodiodes detect the two self-mixing signals without crosstalk. As the source, we were able to use a diode-pumped neodymium-doped yttrium vanadate (Nd:YVO_4 laser crystal) with potassium titanyl phosphate (KTP nonlinear crystal) two-color laser of a commercial pointer. With simple processing of the two self-mixing signals, we are able to obtain the interferometric signals $\cos(2ks)$ and $\sin(2ks)$ at 532 nm, from which the unambiguous measurement of arbitrary target displacement follows with counts in units of $\lambda/8$ of the second-harmonic wavelength or 66 nm.**

***Index Terms*— Interferometry, second-harmonic generation (SHG), self-mixing, solid-state lasers.**

I. Introduction

As it is well known, the interferometric measurement of an arbitrary displacement can be carried out by digital processing of self-mixing interferometer (SMI) signal pair, $\cos(2ks)$, and its orthogonal, $\sin(2ks)$, simply by counting the zero crossings of each signal with the up/down polarity of the other [1]. As the functions sin and cos have four crossing per period and the period corresponds to half wavelength, we obtain a digital readout in units of $\lambda/8$ or 79 nm in commercial instruments working with a He–Ne laser; see, for instance, [1] and [2].

On the other side, when just one signal is available, e.g., $\cos(2ks)$, such as when in the case of a diode laser source, we have the ambiguity problem [3], [4], [5], [6], because near $2ks = 0$ or π, we cannot tell if displacement is increasing or decreasing.

A way out is using the diode laser in the moderate feedback regime [7] so as to develop a switching in the distorted cosine waveform, which happens to be upward or downward according to increasing or decreasing displacement [3], but this method requires a relatively narrow range of feedback strength, $1 < C < 4.7$, and, therefore, needs a control on returning field amplitude.

Manuscript received 29 October 2022; accepted 18 November 2022. Date of publication 8 December 2022; date of current version 12 January 2023. The Associate Editor coordinating the review process was Dr. Yang Bai. *(Corresponding author: Riccardo Gotti.)*

The authors are with the Department of Electrical, Computer and Biomedical Engineering, 27100 Pavia, Italy (e-mail: silvano.donati@unipv.it; riccardo.gotti@unipv.it; antonio.agnesi@unipv.it; federico.pirzio@unipv.it).

Digital Object Identifier 10.1109/TIM.2022.3227611

Another method is to access the frequency modulated component of the SMI signal at the optical frequency, which is just $\sin(2ks)$, by means of a narrowband or steep optical filter [8], [9] at the expense of setup complexity, however.

In this article, we propose and analyze, for the first time at the best of our knowledge, an approach based on taking advantage of the simultaneous presence of optical frequencies ω and 2ω, in a solid-state laser with second-harmonic generation (SHG).

The two wavelength signals happen to carry independent self-mixing modulations, and correspondingly, the two signals detected at the receiving port by two separate photodetectors can be brought to the standard form of sin and cos of external path length $2k_2 s$, where wavelength $\lambda_2 = 2\pi/k_2 = 532$ nm is the SHG of $\lambda_1 = 1064$ nm.

With standard digital processing, we can then obtain the displacement measured in steps of $\lambda_2/8 \approx 66$ nm. This is a sizeable improvement also with respect to previously reported distance measurements [10], [11] by self-mixing interferometry.

This article is organized as follows. In Section II, we outline the basic properties and design of the two-frequency SMI. In Section III, we will calculate the signal amplitudes at ω and 2ω. Then, we report on the experimental results in Section IV, and finally, we draw conclusions in Section V.

II. Design of Setup and Signal Processing

First of all, we shall clarify how the self-mixing effect can take place in the second-harmonic field. Indeed, usually we apply the Lamb's equations to describe self-mixing in a class-A laser, such as He–Ne [12], or the Lang–Kobayashi equations [13] to describe self-mixing in a class-B laser, such as the diode laser.

But, the second-harmonic field is just a wavelength-converted radiation field, missing of a real active medium and of an optical cavity, so the question is: what is the suitable description of the interaction with the fraction returning from the target? The answer is the rotating vector addition model (see [7, Fig. 2]), explaining AM and FM modulations of the nonresonant field at 2ω, without the need to specify nor require any active medium nor cavity.

More precisely, an electric field E_2 that is supplied by the SHG process and has a loss, obeys to Adler's equation [14], which is similar to Lamb's equation, and ends up with the well-known AM and FM terms.

In the following, we will calculate the amplitude modulation of both fundamental and second-harmonic components. Considering the photodetected signals at k_1 and at $k_2 = 2k_1$, they are written as follows:

$$I_1 = I_1^{(0)}[1 + m_1 \cos(2k_1 s)]$$
$$I_2 = I_2^{(0)}[1 + m_2 \cos(2k_2 s)]. \quad (1)$$

By ac coupling or a dc component tracking and subtraction, followed by a gain m_2/m_1, we can equalize the two amplitudes and have:

$$S_1 = \cos(2k_1 s) \text{ and } S_2 = \cos(4k_1 s). \quad (2)$$

Now, several strategies are possible to transform S_1 and S_2 of (2) into an orthogonal pair without ambiguity. We have chosen to process S_1 electronically, so as to bring it to become $\cos(4k_1 s)$ and process S_2 optically to become $\sin(4k_1 s)$. The first operation is accomplished by computing $2S_1^2 - 1 = \cos(4k_1 s)$ out of the electronic signal, for example, by means of an analog integrated circuit (IC) multiplier. The second operation is readily done by phase-shifting the second-harmonic signal S_2 respect to the fundamental S_1 simply by means of a glass plate inserted in the optical path, taking advantage of the material dispersion to introduce a differential path length at the two wavelengths. In this way, we obtain the quadrature signal: in case of no extra phase from the setup, such as in (2), a $\lambda_2/8$ phase shift yields $\cos[4k_1(s + \lambda_2/8)] = -\sin(4k_1 s)$.

With the pair $\cos(4k_1 s)$ and $\sin(4k_1 s)$, we can proceed in the conventional way to obtain the variation of distance Δs or displacement in units of $\lambda_1/16$, as shown in the following.

About the source, it has been shown recently that an ordinary green laser pointer, i.e., a compact diode-pumped monolithic neodymium-doped yttrium vanadate (Nd:YVO_4) laser intracavity doubled with a potassium titanyl phosphate (KTP) crystal, can be used for vibrometry measurements exploiting the SMI [15].

Although the pointers tested in the previous study had a filter permanently glued to block the 1064-nm leakage (to comply with laser safety requirements for use in public), we actually need both the 532- and 1064-nm beams to develop our SMI displacement measurement. Luckily, the technology of green pointers readily supplies compact and low-cost two-color lasers pumped by a semiconductor laser, and therefore, we developed our proof-of-concept experiment with a module containing a diode-pumped Nd:YVO_4/KTP laser emitting 60 mW at 532 nm and 10 mW at 1064 nm, a unit with no output low-pass filter.

Worth to note, the two-color unit is a good choice as the source of an SMI instrument, because it is compact and low cost, completely comparable to the diode laser source normally employed [3], and can, therefore, lead to an attractive alternative for SMI displacement measurements.

Both the two-color pointer and another homebuilt nonmonolithic laser confirmed predictions for the $\omega/2\omega$ displacement measurement concept.

The average power of the two-color laser unit was pretty stable over time, apart instability on microsecond time scale due to axial-modes coupling, i.e., the well-known "green problem" [16], which causes the laser to run on alternating single oscillating modes. Luckily, this instantaneous single-mode regime increases coherence length that becomes long enough to cover distances up to 5 m.

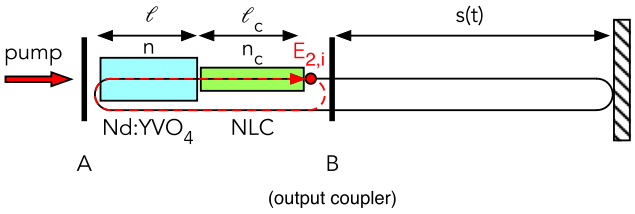

Fig. 1. End-pumped solid-state laser firing on a vibrating target at distance $s(t)$. NLC is the nonlinear crystal. Mirrors A and B are shown separated from crystals but in monolithic devices are actually part of them.

Interestingly, monolithic pointers produce SMI signals robust against microphonic disturbances.

III. Self-Mixing Oscillator With Intracavity SHG

To model our intracavity-doubled four-level laser, we use the well-known Lamb's equation for the fundamental field E_1 [3], [12], [14] that we write in the form

$$t_R \frac{dE_1}{dt} = \frac{1}{2}\left(\frac{g_0}{1 + P/P_S} - L - \eta\right)E_1 + \alpha_1\left(\sqrt{T_1}\right)^2 E_1 \cos(2k_1 s) \quad (3)$$

where g_0 is the round-trip small-signal gain, P_S is the saturation power, $L = L_i + T_1$ is the intracavity fractional loss due to internal contributions L_i and output coupling T_1 at ω (mirror B in Fig. 1), t_R is the round-trip time, α_1 is the target effective reflectivity, and $k_1 = \omega/c$ is the wave vector. The internal SHG efficiency η of these continuous-wave (CW)-pumped lasers usually is proportional to the undepleted fundamental intensity I_1, and it is, therefore, [17]

$$\eta = \frac{\beta I_1^2}{I_1} = \beta I_1 \text{ with } \beta = 8\pi^2 Z_0 \frac{d^2}{n^3 \lambda_1^2} l_c^2 \quad (4)$$

being $Z_0 = (\mu_0/\epsilon_0)^{1/2}$ the vacuum impedance, d the SHG crystal nonlinear coefficient, n the refractive index, and l_c the crystal length. A steady-state condition with no external feedback, i.e., $\alpha_1 = 0$, requires zero net gain

$$\frac{g_0}{1 + P_1/P_S} - L - \beta P_1/A = 0 \quad (5)$$

where P_1 is the circulating intracavity power, and A is the area of the resonant mode, assumed approximately constant in a compact resonator. Equation (5) leads to a second-degree equation [17], which, for a laser operating well above threshold $g_0 \gg L$ and $\beta P_S/A = L$ for optimum SHG, gives

$$P_1^{(0)} \sim \sqrt{\frac{AP_S}{\beta}(g_0 - L)} \text{ and } P_2^{(0)} \sim (g_0 - L)P_S. \quad (6)$$

In practice, output SHG power is basically linearly dependent on pump power through g_0. Assuming weak feedback $\alpha_1 \ll 1$ and using $P_1 = P_1^{(0)} + \Delta P$ in (5), we obtain

$$P_1 \sim P_1^{(0)}\left[1 + 2\alpha_1 \frac{T_1}{g_0}\cos(2k_1 s)\right]$$
$$P_2 \sim P_2^{(0)}\left[1 + 4\alpha_1 \frac{T_1}{g_0}\cos(2k_1 s)\right]. \quad (7)$$

Since it is necessarily $T_1 \ll g_0$, this SMI signal contribution at ω is weak; however, it produces a "feedthrough" modulation, which adds to the expected SMI signal at 2ω with twice the oscillation frequency. The SMI signal at ω detected by a photodiode is usually dominated by the reflection on the external side of mirror B (output coupler), as pointed out in [18]

$$P_1^{(e)} \sim T_1 P_1^{(0)}[1 + 2\alpha_1 \cos(2k_1 s)]. \quad (8)$$

SHG in our case is described by $dE_2/dz = \kappa E_1^2 e^{i\Delta kz}$, where E_1 is approximately constant, $\kappa = Z_0 \omega d/n$, and $\Delta k = k_2 - 2k_1$ is the phase mismatch in the crystal. By integration, we get

$$E_2(l_c) = E_2(0) + \kappa E_1^2 l_c e^{i\Delta k l_c/2} \mathrm{sinc}(\Delta k l_c/2) \quad (9)$$

which shows that the initial field $E_2(0)$ simply adds to the harmonic field generated in a single pass through the crystal, starting from zero input.

Let us now calculate the field at 2ω after one complete round trip in the cavity. Assume $E_{2,i}$ is the field just before output mirror B (red dot in Fig. 1). $E_2^{(-)} = [(R_{2B})^{1/2} E_{2,i} + E_2^{(0)} e^{i\delta}] e^{ik_2(n_{c2}l_c + n_2 l)}$ is the new field after propagation from mirror B to mirror A, being $E_2^{(0)} = \kappa E_1^2 l_c \mathrm{sinc}(\delta)$, and $\delta = \Delta k l_c/2$. Eventually, after propagation from A to B, $E_2^{(+)} = [(R_{2A})^{1/2} E_2^{(-)} e^{ik_2 n_2 l} + E_2^{(0)} e^{i\delta}] e^{ik_2 n_{c2} l_c}$ is the new field at the initial position of $E_{2,i}$. $R_{2A,B}$ is the power reflectivity at 2ω for mirrors A and B, respectively. Therefore, the amplitude change $\Delta E_2 = |E_2^{(+)}| - E_{2,i}$ after one complete round trip without external feedback from the target is

$$\Delta E_2 = \left| \sqrt{R_{2A}} \left(\sqrt{R_{2B}} E_{2,i} + E_2^{(0)} e^{i\delta} \right) e^{i2k_2(n_2 l + n_{c2} l_c)} + E_2^{(0)} e^{i(\delta + k_2 n_{c2} l_c)} \right| - E_{2,i}. \quad (10)$$

The resonating mode at frequency ω satisfies the condition $k_1 n_1 l + k_1 n_{c1} l_c = m\pi$; hence, $2k_2(n_1 + \Delta n)l + 2\ k_2 (n_{c1} + \Delta n_c) l_c = 4\ \mathrm{m}\pi + \phi$ being $\phi = 4k_1 \Delta n l + 4\delta$, where Δn is the dispersion $n_2 - n_1$ in the laser crystal, and Δn_c is the dispersion in the nonlinear crystal (NLC), respectively. Then, we get

$$\Delta E_2 = \left| \sqrt{R_{2A}} \left(\sqrt{R_{2B}} E_{2,i} + E_2^{(0)} e^{i\delta} \right) e^{i\phi} + E_2^{(0)} e^{i\phi_c} \right| - E_{2,i}. \quad (11)$$

Here, phase ϕ includes microphonic effects in nonmonolithic lasers (cavity length fluctuations are included in l), whereas $\phi_c = \delta + k_2 n_{c2} l_c$ is constant (apart slow thermal drifts). It is easier to consider the situation $R_{2A} \approx R_{2B} \ll 1$ (bidirectional green output, such as in our homebuilt nonmonolithic laser), which yields $\Delta E_2 \approx |E_2^{(0)}| - E_{2,i}$. The equation for the second-harmonic field evolution in the presence of an external disturbance (feedback) contains the unperturbed solution $E_2 = \kappa E_1^2 l_c |\mathrm{sinc}(\delta)|$, that is,

$$t_R \frac{dE_2}{dt} \sim \left[\kappa E_1^2 l_c |\mathrm{sinc}(\delta)| - E_2 \right] + \alpha_2 T_{2B} \sqrt{R_{2A}} E_2 \cos(4k_1 s + \phi). \quad (12)$$

Thus, it is similar to the Lamb's equation, despite the conceptual difference, because the active medium is missing. Assuming again small feedback and $T_{2B} \approx 1$, the modulated field at 2ω is

$$E_2 \sim \kappa E_1^2 l_c |\mathrm{sinc}(\delta)| \left[1 + \alpha_2 \sqrt{R_{2A}} \cos(4k_1 s + \phi) \right]. \quad (13)$$

Since the resonant fundamental field is also modulated because of the feedback (7), the SMI signal at 2ω will carry two contributions

$$P_2 \sim P_2^{(0)} \left[1 + 2\alpha_1 \frac{T_1}{g_0} \cos(2k_1 s) \right] \cdot \left[1 + 2\alpha_2 \sqrt{R_{2A}} \cos(4k_1 s + \phi) \right]. \quad (14)$$

Usually, it is $T_1/g_0 \approx 0.01 < (R_{2A})^{1/2} \approx 0.1 - 1$; therefore, the feedthrough modulation contribution is $<10\%$ of the total SMI signal at 2ω. Furthermore, it can be suppressed with high-pass frequency filtering of the $\cos(4k_1 s)$ signal or by subtracting a fraction of signal at ω, which carries $\cos(2k_1 s)$. Another option is to make sure that $\alpha_1 \ll \alpha_2$.

IV. Experiment

Normally, green pointers use the same laser technology, i.e., a Nd:YVO_4 slab and type-II KTP crystal for SHG as in [15], and the elements are glued together to form a monolithic resonator with mirrors directly deposited on end faces.

Also, because of design, end mirrors have high reflectivity at 1064 nm, and mirror B is nearly 100% transmitting at 532 nm. Mirror A is likely highly reflecting at 532 nm.

In our unit, output powers of 60 mW at 532 nm and 10 mW at 1064 nm were measured. Although the self-mixing signal at ω can be independent on T_1 (as pointed out in Section III), sufficient power at 1064 nm is required for successful two-color SMI displacement measurement. In our experiments, we found that the minimum power required for detecting clean self-mixing signals was on the order of 1 mW on each color. To this aim, suitable values of T_1 are in the range of few 0.1% as for typical B-coatings of dichroic mirror (DM).

In the SMI experiment (Fig. 2), a piece of superdiffusing tape (Scotchlite) attached to a loudspeaker driven in the range 10 Hz $< f <$ 100 Hz, far from mechanical resonances, by either a sinusoidal or sawtooth waveform with an amplitude of about 50 mV, yielded few micrometers displacement and, thus, an SMI signal with a reasonably low number of fringes, easy to check for unambiguous counts generation.

A 1-mm BK7 glass beam splitter (BS in Fig. 2) was placed at the output of the laser. The 1064- and 532-nm signals were separated by a DM with a high reflectivity at 532 nm and a high transmissivity at 1064 nm. An infrared-blocking filter F2 (BG38, Schott) was placed in front of the photodiode detecting the 532-nm signal, while a long-pass color filter F1 (FEL1000, Thorlabs) was placed before the other photodiode detecting the 1064-nm signal.

Regarding the detection of the interferometric signal at the two wavelengths, namely, 532 and 1064 nm, two preamplified photodetectors have been realized. Specifically, a Si and an InGaAs p-i-n photodiodes (Hamamatsu S9055 and G3476-03, respectively) were reverse-biased at 10 V and

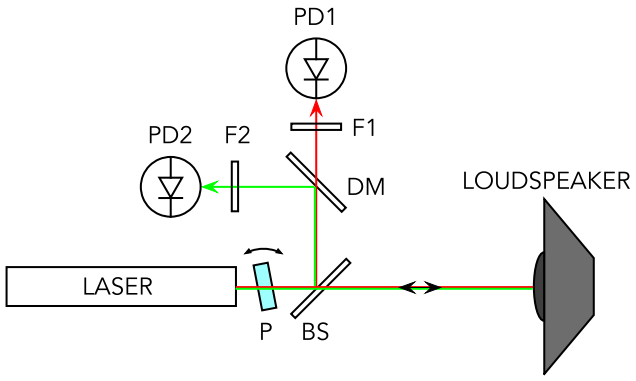

Fig. 2. Experimental setup. BS: glass beam splitter; P: differential phase-shift glass plate; DM: dichroic beam splitter, reflecting green light and transmitting infrared; F1: visible blocking filter; F2: infrared blocking filter; PD1,2: photodiodes detecting infrared and green channels, respectively.

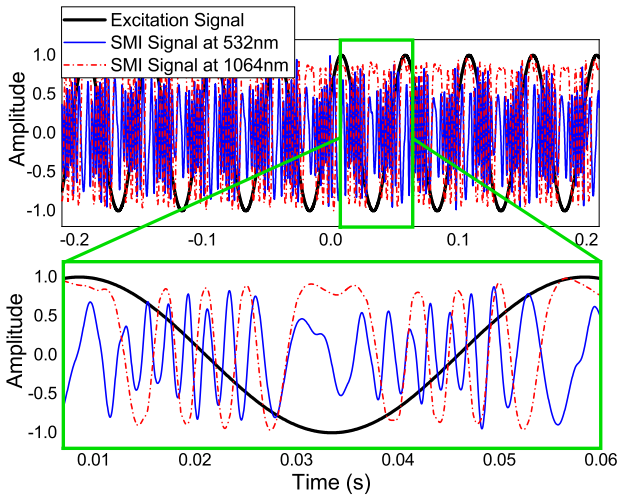

Fig. 3. Top: target excitation signal (black color) and SMI signals after low-pass filtering. Blue color line for the signal $S_2 = \cos(4k_1 s)$ obtained from the 532-nm beam; red color dashed-dotted line for the signal $S_1 = \cos(2k_1 s)$ obtained from the 1064-nm beam. Bottom: zoomed-in view of the three signals.

amplified through operational amplifiers (Texas Instruments TL082) with 10-kΩ transimpedance gain and 3-MHz bandwidth. With impinging (unfocused) signals of about 1 mW, the dc components visible on a 1-MΩ oscilloscope input reached about 2.5 V, while the detection noise remained below 2 mV. In the experimental conditions, the interferometric signals for both wavelengths have amplitude ranging from about 20 to 200 mV around the dc value when using either monolithic (pointers) or nonmonolithic laser sources. This allowed displacement measurements up to ≈5-m target distance.

At present, the bandwidth of our photodetectors is $B \approx 10$ kHz; therefore, the maximum speed of the target is limited to $B\lambda_2/8 \approx 0.66$ mm/s. However, with a refined design, the preamplifier could be improved to $B \approx 1$ MHz, and the speed would reach a reasonable 66 mm/s for a practical instrument.

To demonstrate correct performance with direction discrimination, we acquired simultaneously the two interferometric signals at frequencies ω and 2ω previously introduced as $S_1 = \cos(2k_1 s)$ and $S_2 = \cos(4k_1 s)$, respectively. The acquired experimental signals are shown in Fig. 3 when the target displacement was about ± 1 μm at 20-Hz vibration frequency. The peak-to-peak amplitude of the SMI signal was found stable to <1% on a period of several minutes, and the baseline drift was less than 1% of the peak-to-peak amplitude.

Signal processing was carried out with LabVIEW, in order to fully simulate the operation of the real hardware. The first step consists in the removal of high-frequency noise on the traces through a digital low-pass filter with a cutoff frequency at 1.5 kHz. The next processing step was obtaining the new synthetic signal $C = 2S_1^2 - 1 = \cos(4k_1 s)$, from S_1, to be compared with a phase-shifted S_2, i.e., $S = -\sin(4k_1 s)$.

The latter can be done by adding a thin glass slab, properly tilted, to phase shift S_2 with respect to S_1 by the desired amount to produce a quadrature signal: we used a 1-mm BK7 plate for this (P in Fig. 2). With a tilt angle as small as few degrees, we readily introduced the appropriate differential phase shift in the two beams, also compensating for the contribution introduced by the BS (itself a BK7 plate) of Fig. 2. The glass slab acts as a multiple-order wave plate, but it is quite stable in a temperature range of several degrees °C.

The resulting signals C and S are shown in Fig. 4(a). The orthogonal pair C, S as a function of $4k_1 s$ allows the determination of both the value and the direction of the target displacement $\Delta s(t) = s_0 \cos(2\pi f t)$ with respect to rest position.

Indeed, a logic signal U for forward ($U = 1$) or backward ($U = 0$) motion can be set up by the simultaneous analysis of the amplitudes A_C and A_S, and slopes S_C and S_S, in the C and S signals reported in Fig. 4(a). The result is $U = A_C \oplus S_S + \bar{A}_S \oplus S_C$, where $\oplus$ is the XOR operator, and $\bar{A}_S$ is the negate of A_S, as shown in Fig. 4(d), for consecutive semi-intervals of the loudspeaker excitation wave.

Displacement counts are reported in Fig. 4(c), derived from Fig. 4(b) and from the slopes S_S and S_C (not shown in this figure): there are 33 in each direction, in units of $\lambda_1/16 \approx 66$ nm, for a vibration amplitude $s_0 \approx 1.1$ μm.

It is worth noticing that the nonlinear function C is more sensitive to disturbances and is responsible of fast artifacts in the generated logic signals A_C and S_C. Similarly, spurious artifacts may happen also in A_S and S_S. These are readily suppressed by a digital low-pass filter with 5-kHz cutoff followed by a threshold discriminator. Fig. 4(e) shows the accumulated up/down 66-nm counts for a sinusoidal wave displacement $s(t)$.

The result of Fig. 4(e) has to be understood as exemplary of a displacement measurement, but it is by no way the upper amplitude limit (or dynamic range) of the measurement. Indeed, the SMI signals were detected up to a few meter distances, but the lack of suitable translation stage prevented us from extending the displacement measurements well above the amplitude of Fig. 4(e).

All the signal processing outlined above can be readily carried out also with standard analog/digital circuits or by a dedicated reduced instruction set computer (RISC) or Arduino computer, fed by an analog to digital converter (ADC).

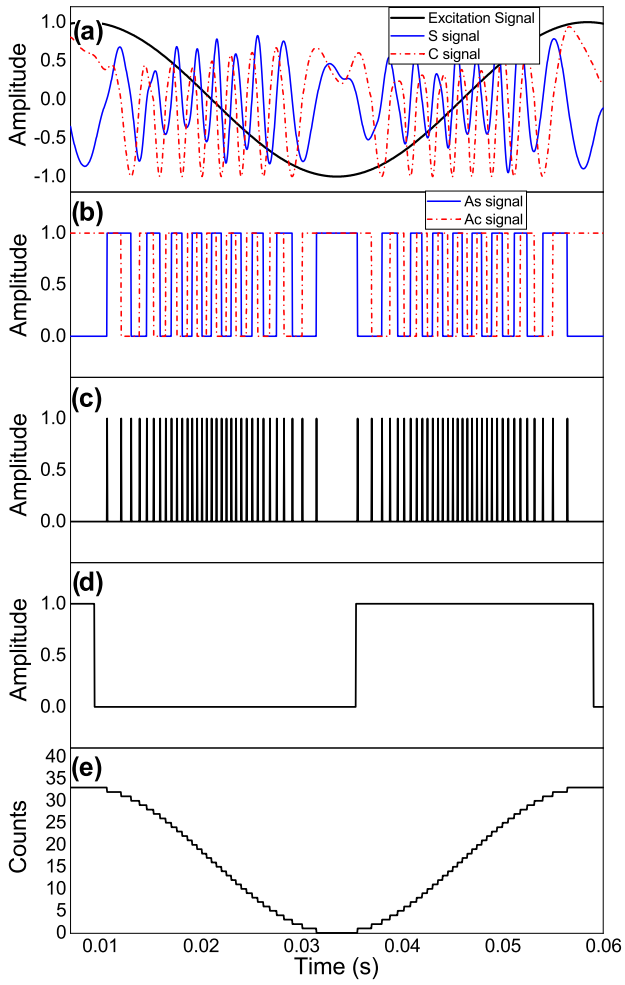

Fig. 4. (a) Loudspeaker and processed signals $S = -\sin(4k_1 s)$ (blue) and $C = 2S_1^2 - 1 = \cos(4k_1 s)$ (red dashed-dotted lines) (zoomed-out portion as in Fig. 3). (b) Boolean signals for amplitudes A_S and A_C. Slope signals S_S and S_C are omitted for clarity. Spurious high-frequency signals are suppressed with low-pass filtering and threshold discrimination. (c) Displacement counts (33 in each direction) in units $\lambda_1/16 \approx 66$ nm. (d) Boolean signal U corresponding to forward (1) and backward (0) target motion. (e) Displacement resulting from up/down counting of pulses in (c), corresponding to a total of ≈ 2.2 μm in each direction.

We investigated the effect of the target distance on the parameter m [(1) of the SMI signal], namely, the modulation amplitude peak-to-peak divided over the dc voltage at the photodetector's output. As can be seen in Fig. 5, the contrast at both wavelengths decreases with increasing target separation with a trend $\approx 1/s$. Thus, even at a target distance of 5 m, the SMI signal is still visible in our setup: this proves that the two-color SMI instrument can work on a span of a few meters.

As a matter of fact, all above findings were confirmed also with two other laser sources: a single-λ 532-nm monolithic pointer of a commercial supplier (following the measurements of [15]) and a homebuilt two-λ table-mounted intracavity-doubled laser.

Indeed, in order to check that the operating principle of the proposed two-color SMI was not tied to a particular design, we built a compact intracavity doubled laser, based on a 3-mm long, 1%-at doped a-cut Nd:YVO_4 crystal and an 8-mm long

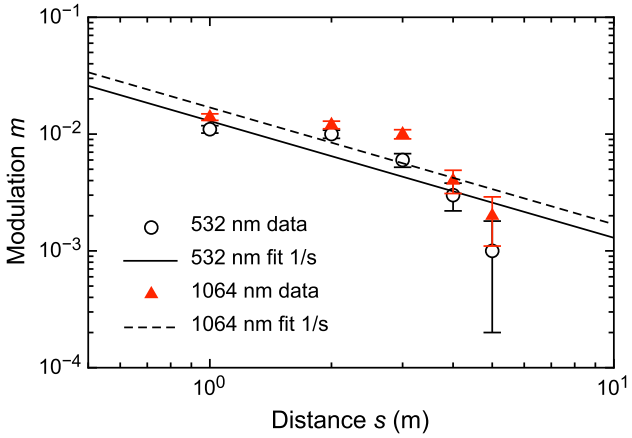

Fig. 5. Dependence of the modulation contrast of the SMI signal with respect to the target distance for the monolithic two-color laser pointer.

lithium triborate (LBO) crystal for type-I SHG, antireflection coated on both sides at ω and 2ω. We set up a 16-mm long plane-plane cavity with high-reflectivity mirrors at 1064 nm on both ends (one end mirror was the coated face of the laser crystal).

The pump was a 1-W multimode laser diode emitting at 808 nm, focused into the laser crystal to a spot radius of about 30 μm allowing TEM_{00} operation. Without the LBO crystal, the laser emitted about 220 mW with a 1%-transmittivity output coupler. With the LBO crystal angle-phase-matched for SHG and the output mirror with transmittivity $T_1 \approx 0.1\%$, the laser emitted about 1 mW at 532 nm (in each direction, since $R_{2A} \approx R_{2B} \approx 5\%$–$10\%$) and 5 mW at 1064 nm. With respect to KTP, the type-I phase matching of LBO produces a linearly polarized beam, while with the KTP, the polarization is generally elliptic [19]. The nonlinearity of LBO is about 1/3 that of KTP, which accounts for the poor SHG efficiency in our case.

We remark that, while the commercial monolithic lasers displayed a very reproducible SMI signal at 532 and 1064 nm (for the two-color pointer), the signals produced by our table-mounted laser were affected by a marked microphonic disturbance, due to the phase ϕ in the term $\cos(4k_1 s + \phi)$ of (13).

All the tested lasers operated reliably in TEM_{00} mode. A laser spectrum was checked with a 1-mm etalon coated for 95% reflectivity at 532 nm: in all cases, we detected two or three longitudinal modes spaced by 40–70 GHz, which is much larger than the resonator-free spectral range, and occasionally even ran with a single axial mode. The number of axial modes detected at 532 nm was confirmed by a near-infrared optical spectrum analyzer (Yokogawa ANDO AQ6317B) around 1064 nm. Fig. 6 shows an example of frequency spectrum.

From Fig. 6, we see that the laser wavelength of the fundamental component jumps on μs time scale from $\lambda = 1063.7$ nm to $\lambda = 1063.8$ nm. Thus, the accuracy of wavelength calibration of the displacement measurement is presently limited to one part in 10^4, but further study may improve this result.

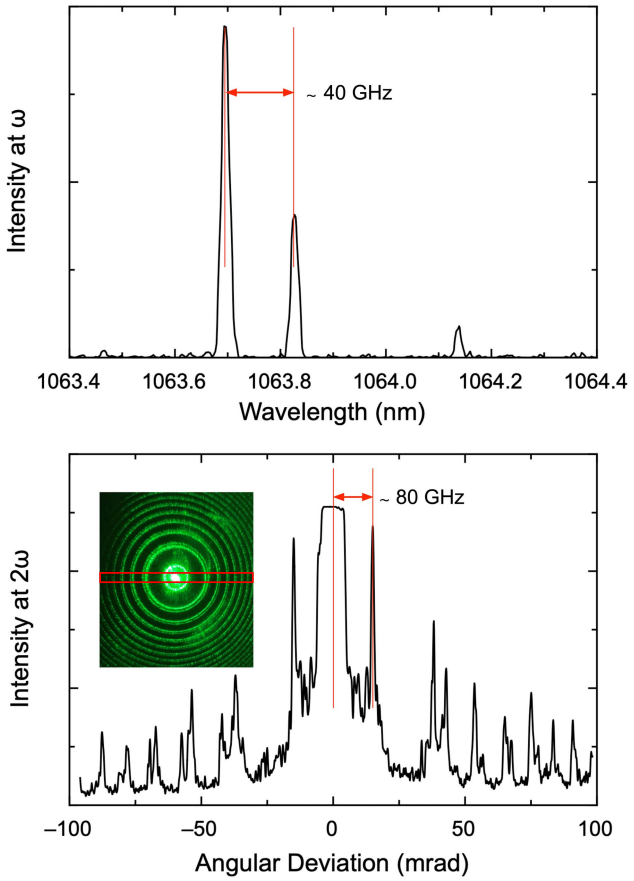

Fig. 6. Top: infrared spectrum of the SMI laser, detected with optical spectrum analyzer (two dominant fundamental modes separated by 40 GHz, and alternatively oscillating, one at the time). Bottom: frequency spectrum at 532 nm detected with 1-mm etalon (inset with rings), confirming there is no significant SFG. The same holds for the two most intense lines in the infrared, with consistent separation.

The amplification bandwidth of Nd:YVO_4 is about 210 GHz [20]: the measured wide axial mode separation is due to spatial hole burning (SHB) [21], which is responsible of a inhomogeneous broadening and allows oscillation of few axial modes with spacing $\Delta\nu_{\mathrm{SHB}} \approx c/(n^2 l_a)$, being the pump absorption length $l_a \approx 1$ mm and the refraction index $n \approx 2$, in fair agreement with observations.

Sum-frequency generation (SFG) is known to cause switching between such axial modes in an intracavity-doubled laser, which always runs on a single mode apart the brief transitory during which the mode hop occurs [16]. This is consistent with the measured coherence length >5 m. When our lasers ran single-axial mode spontaneously for some time, the SMI amplitude was maximum, whereas it was moderately reduced with multiaxial-mode oscillation. It is worth noting that the axial mode pattern, as well as the output power at both wavelengths, has a significant dependence on temperature, which influences cavity length, phase matching, and Lyot filtering produced by the combination of the type-II KTP crystal and the birefringent Nd:YVO_4 [22], [23]. These effects are especially relevant in relatively high-power pointers, with uncontrolled temperature of the laser assembly. Indeed, the lower power monochromatic green pointer produced SMI signals more stable in time.

V. Conclusion

For the first time to the best of our knowledge, we have proposed and demonstrated a two-color SMI with intracavity-doubled diode-pumped solid-state lasers. Experiments with both monolithic and table-mounted miniature resonators have confirmed the SMI signals and the $\lambda_2/8 \approx 66$-nm resolution of our unambiguous displacement measurement. We have backed the experiment with a simple analytic model for the physics of our SMI, highlighting aspects, such as microphonic effects in nonmonolithic sources, confirming the experimental findings.

References

[1] S. Donati, *Electro-Optical Instrumentation*. Upper Saddle River, NJ, USA: Prentice-Hall, 2004.
[2] S. Donati and M. Norgia, "Overview of self-mixing interferometer applications to mechanical engineering," *Opt. Eng.*, vol. 57, no. 5, Mar. 2018, Art. no. 051506.
[3] S. Donati, G. Giuliani, and S. Merlo, "Laser diode feedback interferometer for measurement of displacements without ambiguity," *IEEE J. Quantum Electron.*, vol. 31, no. 1, pp. 113–119, Jan. 1995.
[4] M. C. Amman, T. Bosch, M. Lescure, R. Myllyla, and M. Rioux, "Laser ranging: A critical review of usual techniques for distance measurements," *Opt. Eng.*, vol. 40, no. 1, pp. 10–19, 2001.
[5] S. Donati and S. Merlo, "A PC-interfaced, compact laser-diode feedback interferometer for displacement measurements," *IEEE Trans. Instrum. Meas.*, vol. 45, no. 6, pp. 942–947, Dec. 1996.
[6] M. Norgia and S. Donati, "A displacement-measuring instrument utilizing self-mixing interferometry," *IEEE Trans. Instrum. Meas.*, vol. 52, no. 6, pp. 1765–1770, Dec. 2003.
[7] S. Donati, "Developing self-mixing interferometry for instrumentation and measurements," *Laser Photon. Rev.*, vol. 6, no. 3, pp. 393–417, 2012.
[8] S. Donati and M. Norgia, "Self-mixing interferometer with a laser diode: Unveiling the FM channel and its advantages respect to the AM channel," *IEEE J. Quantum Electron.*, vol. 53, no. 5, pp. 1–10, Oct. 2017.
[9] M. Norgia, V. Contreras, and S. Donati, "Noise in an FM-converted self-mixing interferometer," *IEEE Trans. Instrum. Meas.*, vol. 69, no. 7, pp. 5100–5106, Jul. 2020, doi: 10.1109/TIM.2019.2957867.
[10] M. Norgia, G. Giuliani, and S. Donati, "Absolute distance measurement with improved accuracy using laser diode self-mixing interferometry in a closed loop," *IEEE Trans. Instrum. Meas.*, vol. 56, no. 5, pp. 1894–1900, Oct. 2007.
[11] F. Vogel and B. Toulouse, "A low-cost medium-resolution rangefinder based on the self-mixing effect in a VCSEL," *IEEE Trans. Instrum. Meas.*, vol. 54, no. 1, pp. 428–431, Feb. 2005.
[12] S. Donati, "Laser interferometry by induced modulation of cavity field," *J. Appl. Phys.*, vol. 49, no. 2, pp. 495–497, 1978.
[13] R. Lang and K. Kobayashi, "External optical feedback effects on semiconductor injection laser properties," *IEEE J. Quantum Electron.*, vol. QE-16, no. 3, pp. 347–355, Mar. 1980.
[14] S. Donati and S.-K. Hwang, "Chaos and high-level dynamics in coupled lasers and their applications," *Prog. Quantum Electron.*, vol. 36, nos. 2–3, pp. 293–341, Mar./May 2012.
[15] S. Donati and W. S. Tsai, "Transforming a green laser pointer in a self-mixing interferometer capable of submicrometer vibration sensing," *Appl. Opt.*, vol. 60, no. 21, pp. 6251–6254, 2021.
[16] T. Baer, "Large-amplitude fluctuations due to longitudinal mode coupling in diode-pumped intracavity-doubled Nd:YAG lasers," *J. Opt. Soc. Amer. B, Opt. Phys.*, vol. 3, no. 9, pp. 1175–1180, 1986.
[17] R. G. Smith, "Theory of intracavity optical second-harmonic generation," *IEEE J. Quantum Electron.*, vol. QE-6, no. 4, pp. 215–223, Apr. 1970.
[18] E. M. Randone and S. Donati, "Self-mixing interferometer: Analysis of the output signals," *Opt. Exp.*, vol. 14, no. 20, pp. 9788–9796, 2006.
[19] H. F. Lin, W. Z. Zhu, F. B. Xiong, and H. X. Shen, "An efficient and high polarized single cavity Nd:YVO_4 microchip laser," *Appl. Phys. B, Lasers Opt.*, vol. 111, no. 3, pp. 453–456, May 2013.
[20] W. Koechner, *Solid-State Laser Engineering*, 6th ed. New York, NY, USA: Springer, 2006.
[21] G. J. Kintz and T. Baer, "Single-frequency operation in solid-state laser materials with short absorption depths," *IEEE J. Quantum Electron.*, vol. 26, no. 9, pp. 1457–1459, Sep. 1990.

[22] D. Shen, A. Liu, J. Song, and K. Ueda, "Efficient operation of an intracavity-doubled Nd:YVO_4/KTP laser end pumped by a high-brightness laser diode," *Appl. Opt.*, vol. 37, no. 33, pp. 7785–7788, 1998.
[23] C. Jung, B. A. Yu, I. S. Kim, Y. L. Lee, N. E. Yu, and D. K. Ko, "A linearly-polarized Nd:YVO_4/KTP microchip green laser," *Opt. Exp.*, vol. 17, no. 22, pp. 19611–19616, 2009.

Silvano Donati (Life Fellow, IEEE) was the Chair Professor with the University of Pavia, Pavia, Italy, from 1980 to 2012, where has been an Emeritus Professor since 2015. He has been invited as a Visiting Professor at several Universities of Taiwan: National Taiwan University (NTU), Taipei City, Taiwan, in 2005, National Sun Yat-sen University, Kaohsiung, Taiwan, in 2007, 2008, and 2010, National Cheng Kung University (NCKU), Tainan City, Taiwan, in 2012, National Chung Hsing University (NCHU), Taichung City, Taiwan, from 2013 to 2014, and the National Taipei University of Technology (NTUT), Taipei City, from 2015 to 2016. He has introduced self-mixing interferometry and chaos-shift-keying cryptography, the topics covered in his Distinguished Lecture talk given in 21 Laser and Electro-Optical Society (LEOS) [now Photonics Society (PhoS)] Chapters in two terms, 2007/08 and 2008/09. He has authored or coauthored more than 350 papers and holds 12 patents. He has authored two books, *Photodetectors* (2nd ed. Wiley and IEEE Press, 2020) and *Electro-Optical Instrumentation* (Prentice Hall, 2004).

Prof. Donati is an Optica [formerly Optical Society of America (OSA)] Emeritus Fellow and Society of Photo-Optical Instrumentation Engineers (SPIE) Life Member. He has received several awards from the Associazione Italiana di Elettrotecnica, Elettronica, Automazione, Informatica e Telecomunicazioni (AEIT) and IEEE, in particular the Marconi Medal of AEIT, the Aaron Kressel Award, and the Distinguished Service Award of the IEEE Photonics Society. He was the Founder in 1996 and the first Chair person from 1997 to 2001 of the Italian LEOS Chapter, the LEOS vice president (VP) Region 8 Membership from 2002 to 2004 and Board of Governors (BoG) from 2004 to 2006, and the Chairman of the IEEE Italy Section from 2008 to 2009.

Riccardo Gotti received the degree in engineering physics and the Ph.D. degree in Physics from the Politecnico di Milano, Milan, Italy, in 2014 and 2018, respectively.

He joined the Department of Electrical, Computer and Biomedical Engineering (University of Pavia), Pavia, Italy, as a Junior Assistant Professor, in 2021. His teaching activity involves courses in classical mechanics for engineering students. He has coauthored 32 publications, including peer-reviewed international journals and contributions at national and international conferences. His research interests include molecular spectroscopy with ultrafast frequency combs and high-finesse cavities, and design and use of dedicated optoelectronic and sophisticated laser equipment. His present interests focus on ultrafast laser development and general sensing aspects.

Antonio Agnesi received both the degree in electronic engineering, in 1998, and the Ph.D. degree in electronic engineeriing from the University of Pavia, Pavia, Italy, in 1992.

He was an Associate Professor from 2000 to 2018. He joined the Department of Electrical, Computer and Biomedical Engineering, Pavia, as an Assistant Professor, in 1994. He is currently a Full Professor of physics and has been leading the Laser Sources Laboratory since 2015. His teaching duties include introductory physics courses for engineering students and advanced photonics courses for graduate students. He is also the Co-Founder and Board member of the successful spin-off company Bright Solutions, Via degli Artigiani, Cura Carpignano (PV), Pavia, (started in 1998, now more than 60 employees, half of them graduated/Ph.D.s from the Laser Sources Laboratory). He has authored 238 publications (papers, conference proceedings, and book chapters). He holds three patents. His research interests include experiments/modeling of diode-pumped solid-state and fiber lasers, operating in various regimes, such as continuous-wave (CW), Q-switching, mode-locking (picosecond/femtosecond system) and application of nonlinear optics to pulse generation and compression, and frequency conversion techniques.

Federico Pirzio received the degree in electronic engineering and the Ph.D. degree in electronic engineering and computer science from the University of Pavia, Pavia, Italy, in 2003 and 2007, respectively.

From 2011 to 2020, he has been an Assistant Professor. He is currently an Associate Professor of physics. He is responsible for the Laser Sources Laboratory. His teaching activity involves courses in classical mechanics, classical electromagnetism, and quantum electronics for engineering students. He has coauthored about 70 papers on peer-reviewed international journals, about 50 communications at national and international conferences, and two book chapters. His research interests include the design and numerical modeling of diode-pumped solid-state lasers (continuous wave, nanosecond and subnanosecond Q-switching, and picosecond and femtosecond mode locking), nonlinear frequency conversion devices (harmonic generation, parametric down conversion, and stimulated Raman scattering), characterization of new laser materials, and saturable absorbers for ultrafast lasers.

Dr. Pirzio is a member of the research staff. He serves as an Associate Editor of Optica's *Applied Optics* and a referee for the principal peer-reviewed journals in the field of optics and laser physics.

Open Access funding provided by 'Università degli Studi di Pavia' within the CRUI CARE Agreement